

A seven-planet resonant chain in TRAPPIST-1

Rodrigo Luger^{1,2*}, Marko Sestovic³, Ethan Kruse¹, Simon L. Grimm³, Brice-Olivier Demory³, Eric Agol^{1,2}, Emeline Bolmont⁴, Daniel Fabrycky⁵, Catarina S. Fernandes⁶, Valérie Van Grootel⁶, Adam Burgasser⁷, Michaël Gillon⁶, James G. Ingalls⁸, Emmanuël Jehin⁶, Sean N. Raymond⁹, Franck Selsis⁹, Amaury H. M. J. Triaud¹⁰, Thomas Barclay¹¹⁻¹³, Geert Barentsen^{11,12}, Steve B. Howell¹¹, Laetitia Delrez^{6,14}, Julien de Wit¹⁵, Daniel Foreman-Mackey¹, Daniel L. Holdsworth¹⁶, Jérémy Leconte⁹, Susan Lederer¹⁷, Martin Turbet¹⁸, Yaseen Almleaky^{19,20}, Zouhair Benkhaldoun²¹, Pierre Magain⁶, Brett M. Morris¹, Kevin Heng³ and Didier Queloz^{14,22}

The TRAPPIST-1 system is the first transiting planet system found orbiting an ultracool dwarf star¹. At least seven planets similar in radius to Earth were previously found to transit this host star². Subsequently, TRAPPIST-1 was observed as part of the K2 mission and, with these new data, we report the measurement of an 18.77 day orbital period for the outermost transiting planet, TRAPPIST-1 h, which was previously unconstrained. This value matches our theoretical expectations based on Laplace relations³ and places TRAPPIST-1 h as the seventh member of a complex chain, with three-body resonances linking every member. We find that TRAPPIST-1 h has a radius of 0.752 R_{\oplus} and an equilibrium temperature of 173 K. We have also measured the rotational period of the star to be 3.3 days and detected a number of flares consistent with a low-activity, middle-aged, late M dwarf.

The star TRAPPIST-1 (EPIC 246199087) was observed for 79 days by NASA's Kepler Space Telescope in its two-reaction wheel mission⁴ (K2) as part of Campaign 12, starting on 2016 December 15 and ending on 2017 March 4. The spacecraft was in safe mode between 2017 February 1 and 2017 February 6, resulting in a five-day loss of data. On downlink from the spacecraft, the raw cadence data are typically calibrated with the Kepler pipeline⁵, a lengthy procedure that includes background subtraction, smear removal, and undershoot and non-linearity corrections. However, given the unique science drivers in this dataset, the raw, uncalibrated data for Campaign 12 were made publicly available on 2017 March 8, shortly after downlink. We download and calibrate the long cadence (exposure time $t_{\text{exp}} = 30$ min) and short cadence ($t_{\text{exp}} = 1$ min) light curves

using a simple column-by-column background subtraction, which also removes smear and dark noise (see Methods). Because of its two failed reaction wheels, the rolling motion of the Kepler spacecraft due to torque imbalances introduces strong instrumental signals, leading to an increase in photometric noise by a factor of about three to five compared with the original mission. As TRAPPIST-1 is a faint M8 dwarf with Kepler magnitude $Kp \approx 16-17$ (see Methods), these instrumental signals must be carefully removed to reach the $\sim 0.1\%$ relative photometric precision required to detect Earth-size transits⁶. To this end, we detrend the long cadence light curve for TRAPPIST-1 using both EVEREST^{7,8} and a Gaussian process-based pipeline, achieving an average 6h photometric precision of 281.3 ppm, a factor of three improvement over the raw light curve. After analysis of the long cadence light curve, we detrend the short cadence light curve in the vicinity of the features of interest, achieving a comparable or higher 6h precision (see Methods).

We conduct three separate transit searches on the long cadence light curve, aiming to constrain the period of TRAPPIST-1 h, which had only been observed to transit once², and to detect additional planets in the system. A dynamical analysis made by our team before the release of the K2 data suggested certain values of the period of TRAPPIST-1 h based on the presence of three-body resonances among the planets. Three-body resonances satisfy $pP_1^{-1} - (p+q)P_2^{-1} + qP_3^{-1} \approx 0$ and $p\lambda_1 - (p+q)\lambda_2 + q\lambda_3 = \phi$ for integers p and q where P_i and λ_i are the period and mean longitude of the i th planet^{9,10} and ϕ is the three-body angle, which librates about a fixed value. Such resonances occur both in our Solar System—the archetypical case being the Laplace resonance among Jupiter's

¹Astronomy Department, University of Washington, Seattle, Washington 98195, USA. ²NASA Astrobiology Institute's Virtual Planetary Laboratory, Seattle, Washington 98195, USA. ³University of Bern, Center for Space and Habitability, Sidlerstrasse 5, CH-3012 Bern, Switzerland. ⁴Laboratoire AIM Paris-Saclay, CEA/DRF-CNRS-Université Paris Diderot, IRFU/SAP Centre de Saclay, 91191 Gif-sur-Yvette, France. ⁵Department of Astronomy and Astrophysics, University of Chicago, 5640 South Ellis Avenue, Chicago, Illinois 60637, USA. ⁶Space Sciences, Technologies and Astrophysics Research Institute, Université de Liège, Allée du 6 Août 19C, B-4000 Liège, Belgium. ⁷Center for Astrophysics and Space Science, University of California San Diego, La Jolla, California 92093, USA. ⁸IPAC, Mail Code 314-6, California Institute of Technology, 1200 East California Boulevard, Pasadena, California 91125, USA. ⁹Laboratoire d'Astrophysique de Bordeaux, Université Bordeaux, CNRS, B18N, allée Geoffroy Saint-Hilaire, 33615 Pessac, France. ¹⁰Institute of Astronomy, Madingley Road, Cambridge CB3 0HA, UK. ¹¹NASA Ames Research Center, Moffett Field, California 94043, USA. ¹²Bay Area Environmental Research Institute, 25 2nd Street Ste 209 Petaluma, California 94952, USA. ¹³NASA Goddard Space Flight Center, Greenbelt, Maryland 20771, USA. ¹⁴Cavendish Laboratory, J.J. Thomson Avenue, Cambridge CB3 0HE, UK. ¹⁵Department of Earth, Atmospheric and Planetary Sciences, Massachusetts Institute of Technology, 77 Massachusetts Avenue, Cambridge, Massachusetts 02139, USA. ¹⁶Jeremiah Horrocks Institute, University of Central Lancashire, Preston PR1 2HE, UK. ¹⁷NASA Johnson Space Center, 2101 NASA Parkway, Houston, Texas 77058, USA. ¹⁸Laboratoire de Météorologie Dynamique, Sorbonne Universités, UPMC Université Paris 06, CNRS, 4 place Jussieu, 75005 Paris, France. ¹⁹Space and Astronomy Department, Faculty of Science, King Abdulaziz University, 21589 Jeddah, Saudi Arabia. ²⁰King Abdullah Centre for Crescent Observations and Astronomy, Makkah Clock, Mecca 24231, Saudi Arabia. ²¹LPHEA Laboratory, Oukaïmeden Observatory, Cadi Ayyad University FSSM, BP 2390 Marrakesh, Morocco. ²²Observatoire de Genève, Université de Genève, 51 chemin des Maillettes, CH-1290 Sauverny, Switzerland. *e-mail: rodluger@uw.edu

satellites, satisfying $(p, q) = (1, 2)$ —and in exoplanet systems, two of which were recently observed to have resonant chains among four planets: Kepler-223¹¹ with $(p, q) = (1, 1)$ and Kepler-80¹² with $(p, q) = (2, 3)$. Among the inner six planets in TRAPPIST-1, there are four adjacent sets of three planets that satisfy this relation for $1 \leq p \leq 2$ and $1 \leq q \leq 3$ (Table 1). This suggested that the period of planet TRAPPIST-1 h may also satisfy a three-body resonance with TRAPPIST-1 f and g. The six potential periods of TRAPPIST-1 h that satisfy three-body relations with $1 \leq p, q \leq 3$ are 18.766 days ($p = q = 1$), 14.899 days ($p = 1, q = 2$), 39.026 days ($p = 2, q = 1$), 15.998 days ($p = 2, q = 3$), 13.941 days ($p = 1, q = 3$) and 25.345 days ($p = 3, q = 2$). We examined ~1,000 h of ground-based data taken before the Spitzer dataset² and found a lack of obvious additional transits at the expected times for all these periods apart from 18.766 days. The period of 18.766 days corresponds to prior transit times in windows that were missed by the previous ground-based campaigns, hence this was the only period that could not be ruled out. As this value is consistent with the period estimate of 20^{+15}_6 day based on the duration of the Spitzer transit, we had reason to believe that it was the correct period for TRAPPIST-1 h. To test this hypothesis, in our first transit search we simply fold the long cadence light curve at the four expected times of transit given this period and the single Spitzer transit time, finding evidence for a transiting planet with that period. Follow-up with detrended short cadence data confirms the transit-like shape of each of the four events and a depth consistent with that of TRAPPIST-1 h (see Methods).

To prove the uniqueness of this detection, in a second analysis we search the detrended K2 light curve after subtracting a transit model including all known transits of planets TRAPPIST-1 b–g, based on published ephemerides and planet parameters². We use the photometric residuals as input to a box-fitting least-squares (BLS) algorithm (see Methods) to search for additional transit signals. In this search, we do not impose prior information on TRAPPIST-1 h. We find a periodic signal at ~18.77 days with a transit centre at Barycentric Julian date (BJD) = 2,457,756.39, which matches the single transit observed by Spitzer².

Independently, we perform a joint instrumental–transit model fit to the data after subtracting a model for planets TRAPPIST-1 b–g based on the Spitzer parameters (see Methods). We compute the relative likelihood ($\Delta\chi^2$) of a transit model with the best-fit Spitzer parameters of TRAPPIST-1 h centred at every long cadence and sum the $\Delta\chi^2$ values at the transit times corresponding to different periods in the range 1–50 days. Strong peaks emerge at 18.766 days and its aliases, corresponding to four transit-like events consistent with the parameters of TRAPPIST-1 h at the times recovered in the previous searches.

We use the orbital period of TRAPPIST-1 h determined in the previous step along with the parameters² of planets TRAPPIST-1 b–g to determine whether a model including TRAPPIST-1 h is favoured. This is achieved through Markov Chain Monte Carlo (MCMC) model fits with and without TRAPPIST-1 h. We find a Bayes factor of 90 in favour of a model that includes TRAPPIST-1 h (see Methods), supporting the photometric detection of this seventh planet in the K2 dataset. The detection of TRAPPIST-1 h is thus supported by: (1) the three transit search analyses that recovered both the orbital phase from the Spitzer ephemeris² and the period of 18.766 days; (2) the Bayes factor in favour of the seven-planet model; and (3) the orbital period that is the exact value predicted by Laplace relations. Figure 1 shows the full light curve, the newly found transits of TRAPPIST-1 h and an update to the geometry of the orbits given the new orbital period. Table 2 reports the properties of the planet derived in this study.

To characterize the three-body resonance, we use the transit timing data to identify ϕ (see Methods) for each set of three planets. A full transit timing cycle has not elapsed within the data, so we cannot estimate the libration centre for each value of ϕ . However, we report in Table 1 the values of ϕ represented in the dataset.

Table 1 | Three-body resonances of TRAPPIST-1.

Planets 1, 2, 3	p	q	$\frac{p}{P_1} - \frac{(p+q)}{P_2} + \frac{q}{P_3}$ (day ⁻¹)	$\phi = p\lambda_1 - (p+q)\lambda_2 + q\lambda_3$
b, c, d	2	3	$(-4.6, -0.3) \times 10^{-5}$	$(176^\circ, 178^\circ)$
c, d, e	1	2	$(-5.2, +4.5) \times 10^{-5}$	$(47^\circ, 50^\circ)$
d, e, f	2	3	$(-1.9, +1.9) \times 10^{-4}$	$(-154^\circ, -142^\circ)$
e, f, g	1	2	$(-1.4, +1.1) \times 10^{-4}$	$(-79^\circ, -72^\circ)$
f, g, h	1	1	$(-6.0, +0.2) \times 10^{-5}$	$(176.5^\circ, 177.5^\circ)$

The transit times are used to track the ϕ angles of each set of three adjacent planets over the dataset, assuming low eccentricities such that transits occur at a phase angle $\lambda = 90^\circ$. The ranges of three-body frequency and angle given encompass the changes—most likely librations—seen during the observations.

In the case of Jupiter’s satellites, $\phi = 180^\circ$, but due to the complexity of this multi-planet system, we make no prediction for TRAPPIST-1 at this time. Migration and damping simulations applied to Kepler-80 (ref. 12) naturally predicted the values of the libration centres in that system; the measured values for TRAPPIST-1 b–h call for future theoretical work to interpret.

The resonant structure of the system suggests that orbital migration may have played a part in its formation. Embedded in gaseous planet-forming disks, planets growing above ~0.1 M_\oplus (approximately the mass of Mars) create density perturbations that torque the planets’ orbits and trigger radial migration¹³. One model for the origin of low-mass planets found very close to their stars proposes that Mars- to Earth-sized planetary embryos form far from their stars and then migrate inwards¹⁴. The inner edge of the disk provides a migration barrier¹⁵ such that the planets pile up into chains of mean motion resonances^{16–18}. This model matches the observed period ratio distribution of adjacent low-mass ($\lesssim 10 M_\oplus$) planets¹⁹ if the majority (~90%) of resonant chains become unstable and undergo a phase of giant impacts²⁰. Some resonant chains do survive and a handful of systems with multiple resonances among low-mass planets have been characterized^{11,21}. The TRAPPIST-1 system may thus represent a pristine surviving chain of mean motion resonances. Given that the planet-forming disk of TRAPPIST-1 was probably low in mass²² and the planets themselves are low mass, their migration was probably relatively slow. This may explain why the resonant chain of TRAPPIST-1 is modestly less compact than chains in systems with more massive planets^{11,20,21}; this may have protected the chain from instability²³.

Tidal interactions are likely to be important in the planets’ orbital evolution, given how close the planets orbit TRAPPIST-1²⁴. Tidal simulations of the system (see Methods) show that the eccentricity of each planet is damped to <0.01 within a few million years. Nonetheless, tidal heating is significant: all planets except TRAPPIST-1 f, g and h have a tidal heat flux higher than Earth’s total heat flux.

The incident stellar flux on planet TRAPPIST-1 h, 200 W m^{-2} , is less than the 300 W m^{-2} required to sustain surface liquid water under an $\text{N}_2/\text{CO}_2/\text{H}_2\text{O}$ atmosphere (see Methods). To obtain the missing 100 W m^{-2} from tidal heating would require a high eccentricity, which is strictly incompatible with the orbits of the other planets. Our simulations show that the stellar input is also too low to sustain a thick CO_2 atmosphere due to CO_2 condensation. In particular, CO_2 levels cannot exceed 100 ppm within a 1 bar N_2 atmosphere. Alternatively, a liquid water ocean is possible under a layer of ice. The minimum thickness h of this layer of ice depends on the internal heat flux ϕ_{int} :

$$h \approx 250 \left(\frac{\phi_{\text{int}}}{1 \text{ W m}^{-2}} \right)^{-1} \text{ m}$$

Assuming the Earth’s current geothermal flux of 0.090 W m^{-2} , a layer of ice 2.8 km thick (the mean depth of Earth’s oceans) would be necessary.

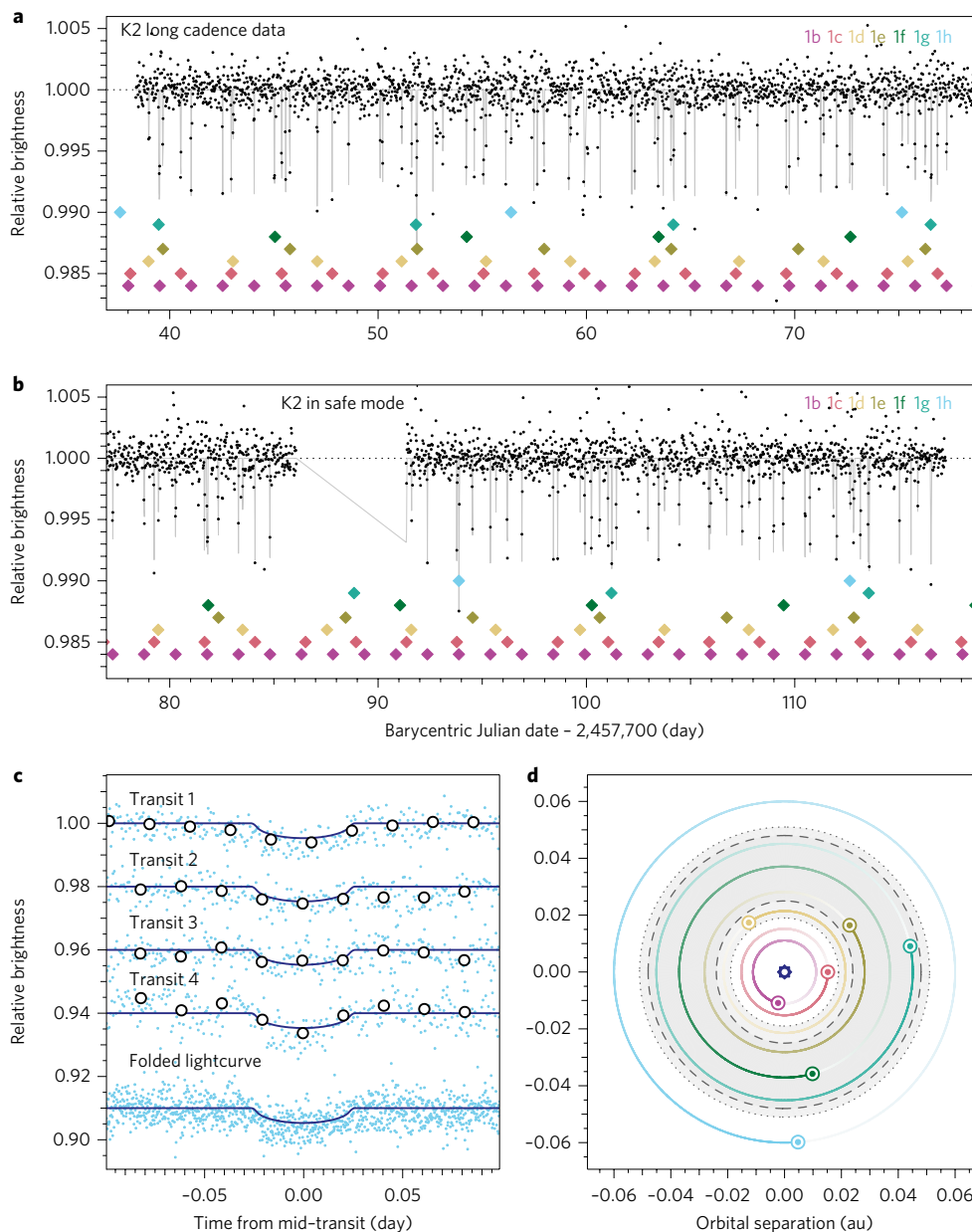


Figure 1 | Long cadence K2 light curve of TRAPPIST-1 detrended with EVEREST. a, The first half of the detrended K2 light curve with stellar variability removed via LOESS regression (order = 1; width = 0.15 day). Data points are in black and our highest likelihood transit model for all seven planets is plotted in thin grey. Coloured diamonds indicate which transit belongs to which planet. Two transits of TRAPPIST-1 h are observed (light blue diamonds). **b**, The second half of the detrended K2 light curve. Two additional transits of TRAPPIST-1 h are visible. **c**, The top four curves show the detrended and whitened short cadence in light blue, with a transit model based on the Spitzer parameters in dark blue. Binned data is over-plotted in white for clarity. The folded light curve is displayed at the bottom. **d**, View from above (observer to the right) of the TRAPPIST-1 system at the date when the first transit was obtained for this system. The grey region is the surface liquid water habitable zone.

Although the long spin-down times of ultracool dwarfs prevent the derivation of a robust gyrochronology relation²⁵, the rotational period of TRAPPIST-1 can be used to derive a provisional age estimate for the system. Fourier analysis of the detrended K2 data (Fig. 2), which is visibly modulated by star spots, leads to the determination of a rotational period of ~ 3.3 days for the host star (see Methods). This rotation corresponds to an angular momentum of $\sim 1\%$ of that of the Sun. It is roughly in the middle of the period distribution of nearby late M dwarfs²⁶, suggesting an age in the range 3–8 Gyr based on a star formation rate that decreases slightly over time²⁷. Such an age is consistent with the star's solar metallicity¹ and borderline thin disk–thick disk kinematics²⁸. The amplitude of the modulation due to star spots and infrequent weak optical flares

(0.26 day^{-1} for peak fluxes $>1\%$ of the continuum, 40 times less frequent than active M6–M9 dwarfs²⁹) are consistent with a low-activity M8 star, also arguing in favour of a relatively old system. An energetic flare erupted near the end of the K2 Campaign and was observed by Kepler. Full modelling of flares will be presented in a forthcoming paper.

The K2 observations of the TRAPPIST-1 star have enabled the detection of the orbital period of TRAPPIST-1 h, continuing the pattern of Laplace resonances among adjacent triplets of planets. We search for, but do not detect, additional planets in the system. Compared with previous ground-based and Spitzer observations, the continuous coverage, high precision and shorter wavelength of the K2 observations enable a robust estimate of the rotational

Table 2 | Properties of TRAPPIST-1 h, limb-darkening parameters and transit timings derived using a joint Spitzer and K2 dataset.

Parameter	Value
Transit depth, $(R_p/R_*)^2$ (%)	0.346 ± 0.018
Transit duration (day)	0.0525 ± 0.0008
Impact parameter, b (R_*)	$0.45_{-0.08}^{+0.06}$
Mid-transit time, T_0 (BJD _{TDB})	$2,457,662.55284 \pm 0.00037$
Period, P (day)	$18.767_{-0.003}^{+0.004}$
Radius ratio, R_p/R_*	0.0588 ± 0.0016
Radius, R_p (R_\oplus)	$0.752_{-0.031}^{+0.032}$
Inclination, i ($^\circ$)	$89.76_{-0.04}^{+0.05}$
Scale parameter, a/R_*	109 ± 4
Equilibrium temperature (K)	173 ± 4
Irradiation, S_p (S_\oplus)	0.165 ± 0.025
Limb-darkening parameters (Kepler bandpass)	
u_1	1.00 ± 0.02
u_2	-0.04 ± 0.04
Individual transit timings from K2 (BJD _{TDB})	
Transit 1	$2,457,756.3874_{-0.0013}^{+0.0013}$
Transit 2	$2,457,775.1539_{-0.0016}^{+0.0016}$
Transit 3	$2,457,793.9230_{-0.0025}^{+0.0024}$
Transit 4	$2,457,812.6987_{-0.0042}^{+0.0045}$

Parameter values are the medians of the posterior distributions from the MCMC and the associated errors are the 1σ credible intervals. R_p is the planet radius and a is the semimajor axis.

period and flare activity of the star, motivating further study of the atmospheres and dynamical evolution of the planetary system.

Methods

Light curve preparation. We use the package *kadenza* to generate a target pixel file from the Campaign 12 raw data for TRAPPIST-1 (see Code availability). In addition to EPIC ID 246199087, which corresponds to a standard-size postage stamp centred on TRAPPIST-1, the Kepler GO Office also made available a larger, 11×11 pixel custom mask with a different ID (200164267), which we use for the purposes of this study. We manually select a rectangular 6×6 pixel ($24'' \times 24''$) aperture centred on TRAPPIST-1 and use the median values of the remaining pixels to perform a column-by-column background subtraction. This process removes dark current and background sky signals while mitigating smear due to bright stars in the same CCD column as the target. Based on simple error function fits to the stellar image, we find that our aperture encloses >0.9996 of the flux of TRAPPIST-1 h throughout the entire time series. We then detrend and perform photometry on the pixel level data using two independent pipelines: EVEREST and a Gaussian process based detrender. For computational expediency, we perform preliminary analyses on the long cadence data, following up on features of interest in the short cadence data.

Light curve detrending using EVEREST. The EVEREST K2 pipeline⁷ uses a variant of pixel level decorrelation³⁰ (PLD) to remove instrumental systematics from stellar light curves. Given a stellar image spread out over a set of pixels $\{p_i\}$, EVEREST regresses on polynomial functions of the fractional pixel fluxes, $p_i/\Sigma_j p_j$, identifying the linear combination of these that best fits the instrumental signals present in the light curve. Because astrophysical signals (such as transits) are equally present in each of the pixels, whereas instrumental signals are spatially variable, PLD excels at removing instrumental noise while preserving astrophysical information. EVEREST uses a Gaussian process to model correlated astrophysical noise and uses an L2-regularized regression scheme to minimize overfitting.

As PLD may overfit in the presence of bright contaminant sources in the target aperture⁷, we manually inspect the TRAPPIST-1 K2 postage stamp and high-resolution images of TRAPPIST-1 taken with the Apache Point Observatory ARC 3.5 m telescope in the Slone Digital Sky Survey z band to verify that there is no other target brighter than the background level in our adopted aperture, consistent with results obtained from Gemini-South speckle imaging of the target³¹. Given the faint magnitude of TRAPPIST-1 in the Kepler band, we use the PLD vectors of 14 nearby bright stars (EPIC IDs 246177238, 246165150, 246211745, 246171759, 246127507, 246228828, 206392586, 246121678, 246229336, 246196866, 24621755,

246239441 and 246144695), generated using the same method, to improve the signal-to-noise ratio of the instrumental model⁸. We further mask the data in the vicinity of all transits of planets TRAPPIST-1 b–g and the potential transits of TRAPPIST-1 h when computing the model to prevent transit overfitting. We then divide the light curve into three roughly equal segments and detrend each separately to improve the predictive power of the model. Following these steps, we obtain a detrended light curve for TRAPPIST-1 with a 6 h photometric precision^{7,32} of 281.3 ppm, a factor of three improvement on that of the raw light curve (884.4 ppm); see Fig. 1. Before the K2 observation, we estimated the Kp magnitude of TRAPPIST-1 to be 17.2 ± 0.3 based on a fit to a corrected blackbody spectrum. However, the photometric precision we achieve with EVEREST is inconsistent with a target dimmer than $Kp \approx 17$. Our detrending therefore suggests that the magnitude of TRAPPIST-1 in the Kepler band is $16 < Kp < 17$.

Light curve detrending using Gaussian process model. Independently, we also detrend the data with a Gaussian process-based pipeline. To perform aperture photometry, we locate the star using a centroid fit and apply a circular top-hat aperture following the star's centroid coordinates. We then use a Gaussian process model to remove the pointing drift systematics using an additive kernel with separate spatial, time and white noise components^{33,34}:

$$k_{xy}(x_i, y_i, x_j, y_j) = A_{xy} \exp \left[-\frac{(x_i - x_j)^2}{L_x^2} - \frac{(y_i - y_j)^2}{L_y^2} \right] \quad (1)$$

$$k_{xy}(t_i, t_j) = A_t \exp \left[-\frac{(t_i - t_j)^2}{L_t^2} \right] \quad (2)$$

$$K_{ij} = k_{xy}(x_i, y_i, x_j, y_j) + k_t(t_i, t_j) + \sigma^2 \delta_{ij} \quad (3)$$

where x and y are the pixel coordinates of the centroid, t is the time of the observation, δ_{ij} is the Kronecker delta and the other variables (amplitudes A_{xy} and A_t , length scales L_x and L_y , timescale L_t and standard deviation σ) are hyperparameters of the Gaussian process model. We use the GEORGE package³⁵ in PYTHON to implement the Gaussian process model. To find the maximum likelihood hyperparameters, we use a differential evolution algorithm³⁶ followed by a local optimization. This method was tested on magnitude 16–18 stars observed in Campaign 10 of K2 and we use the results of those tests, and of previous Gaussian process applications to K2 data³⁴, to inform our priors on the hyperparameters.

For the TRAPPIST-1 data, we use an iterative σ -clipping method to remove outliers and prevent the time component from overfitting. This method has been previously used in the *k2sc* (ref. ³⁴) pipeline. First, using fiducial hyperparameter values based on the analysis of a Campaign 10 target, we remove all measurements with residuals $>3\sigma$ from the mean Gaussian process prediction. With the remaining measurements, we update the hyperparameters by maximizing the Gaussian process likelihood. Using these parameters, we once again clip all 3σ outliers and maximize the Gaussian process likelihood using only the remaining measurements. The final detrending is calculated for all points, including outliers.

Photometric analysis I. We fold the long cadence data on the dynamically predicted orbital period of 18.765 days for TRAPPIST-1 h with a time of first transit constrained by the Spitzer observation, revealing a feature consistent with a transit in both the EVEREST- and Gaussian process-based light curves. To confirm the planetary nature of this signal, we analyse the short cadence data. To this end, we use *kadenza* to generate a short cadence target pixel file of TRAPPIST-1 and detrend it in windows of 1.5–2.0 days centred on each of the four features using EVEREST. We use the PLD vectors of five bright stars observed in short cadence mode (EPIC IDs 245919787, 246011640, 246329409, 246331757 and 246375295) to aid in the detrending. When generating these light curves, we explicitly mask large flares so that these do not inform the fit. Following this procedure, we obtain binned 6 h photometric precisions of 266.6, 176.1, 243.4 and 219.3 ppm in each of the four windows. The short and long cadence data in these windows is shown in Supplementary Fig. 1. Additional correction of the light curve is necessary for transits 3 and 4 because the transit of TRAPPIST-1 h coincides with a transit of TRAPPIST-1 b (panel 3a of Supplementary Fig. 1) and a small flare (panel 4b). The transit of TRAPPIST-1 b is subtracted out using a transit model³⁷ with the Spitzer parameters and a mid-transit time determined from the data, yielding the light curve in panel 3b. The flare is fitted using a three-parameter flare model³⁸ for stars observed with Kepler, yielding the light curve in panel 4b (see also Supplementary Fig. 2). In both cases, the transit of TRAPPIST-1 h is visible in the residuals. In Supplementary Fig. 3 we show the folded short cadence data after accounting for transit timing variations (TTVs), with a transit model based solely on the Spitzer parameters.

Photometric analysis II. We use the long cadence detrended light curve to perform a transit search with a BLS³⁹. We set the BLS to orbital periods ranging from

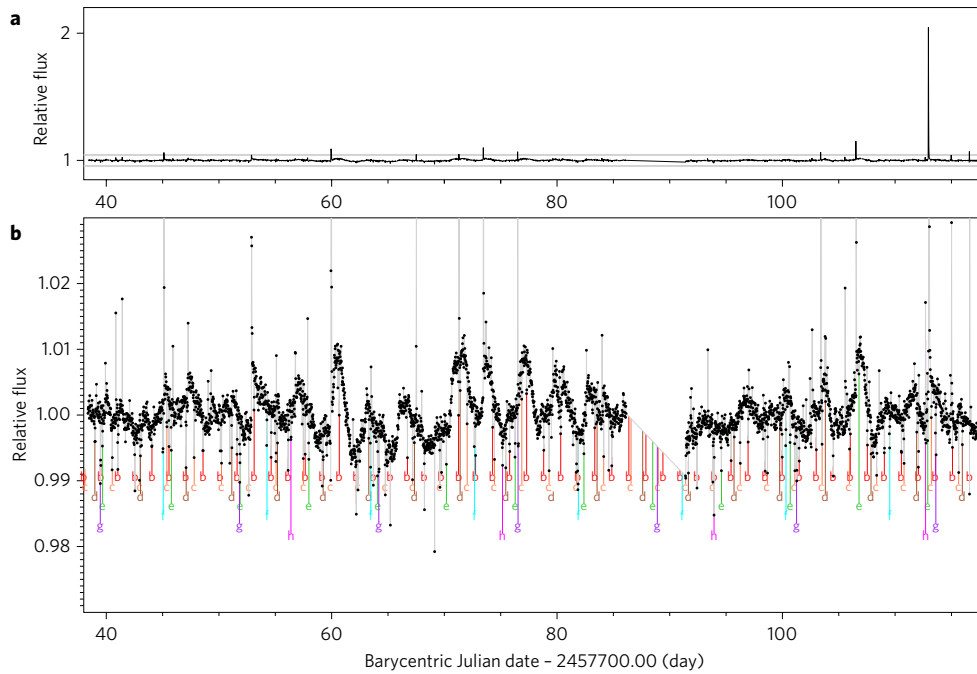


Figure 2 | Entire systematics-corrected K2 dataset with low-frequency trends removed. The stellar rotation is apparent in the peaks and troughs of the variability, as are the flares, which, in some cases, appear as single spikes. The planet transits are marked. **a**, Full dynamic range of the curve, including an extreme event at approximately day 113. **b**, Zoomed view of the region outlined in grey in **a**.

10 to 50 days. The ratio of the transit duration over the planet orbital period is set between 0.0007 and 0.06 to include a wide range of orbital periods, eccentricities and impact parameters for additional planets in the system. As a result of Kepler’s 30 minute cadence, transits of planets orbiting TRAPPIST-1 appear significantly smeared out, which we take into account in our analysis. The highest peak in the periodogram corresponds to a signal with a 15.44 day period. Its origin stems from residuals in blended transits with TRAPPIST-1 c and d and from one outlier in the data. No signal is seen at the two other epochs where a transit should have appeared, which confirms the signal is spurious. The next highest peak in the periodogram corresponds to a ~18.77 day period and a transit centre at BJD = 2,457,756.39, which is consistent with the single transit seen with Spitzer.

We then use an MCMC algorithm⁴⁰ to derive the transit parameters of TRAPPIST-1 h from the detrended light curve. Each photometric data point is attached to a conservative error bar that accounts for the uncertainties in the detrending process presented in the previous section. We impose normal priors in the MCMC fit on the orbital period, transit mid-time centre and impact parameter for planets TRAPPIST-1 b–g to the values recently published². We further assume circular orbits for all planets^{1,2}. We also include normal priors for the stellar properties, which are $\mathcal{N}(0.080, 0.007^2) M_{\odot}$ for the mass, $\mathcal{N}(0.117, 0.004^2) R_{\odot}$ for the radius, $\mathcal{N}(2,555, 85^2) K$ for the effective temperature and $\mathcal{N}(0.04, 0.08^2) dex$ for the metallicity². We use these stellar parameters to compute the quadratic limb-darkening coefficients u_1 and u_2 in the Kepler bandpass from theoretical tables⁴¹. In a first MCMC fit, we use a seven-planet model that includes all seven planets, with no prior information on the orbital period or t_0 (the time of transit) of TRAPPIST-1 h. In the second fit we use a six-planet model that excludes TRAPPIST-1 h. We use the results from both MCMC fits to compute the Bayesian and Akaike information criteria to determine which model is favoured. We find Bayesian information criteria values of 2,888 and 2,897 for the seven- and six-planet models, respectively. This corresponds to a Bayes factor $e^{(BIC_1 - BIC_2)/2} = 90$ in favour of the seven-planet model. Similarly, we find Akaike information criterion values of 2,691 and 2,725 for the seven- and six-planet models, respectively. We perform a third MCMC fit to refine the transit parameters of TRAPPIST-1 h. For this fit, we use as input data the K2 short cadence data centred on the four transits of TRAPPIST-1 h (Fig. 1) and the single transit light curve previously obtained with Spitzer. This fit includes a model for TRAPPIST-1 b and a flare that both affect the transit shape of TRAPPIST-1 h in the K2 short cadence data. This fit also allows for TTVs for the individual transit timings. We find photometric precisions of 365 and ~1,100 ppm per 10 minutes for the Spitzer and K2 data, respectively. We report the median and 1σ credible intervals of the posterior distribution functions for the transit parameters of TRAPPIST-1 h in Table 2, along with the individual transit times.

Photometric analysis III. To prevent the overfitting of transit features, we mask all transits of planets TRAPPIST-1 b–h when detrending with EVEREST.

However, this inevitably results in a lower detrending power during transits. A powerful alternative to this detrend-then-search method is to simultaneously fit the instrumental and transit signals without masking these features⁴². We therefore conduct a second separate blind search on the EVEREST light curve specifically for TRAPPIST-1 h. Given a raw light curve \mathbf{y} , a data covariance matrix Σ and a single transit model \mathbf{m}_{t_0} centred at $t = t_0$, the log likelihood of the transit fit is

$$\log \mathcal{L} = -\frac{1}{2}(\mathbf{y} - \mathbf{m}_{t_0})^T \Sigma^{-1}(\mathbf{y} - \mathbf{m}_{t_0}) + C \quad (4)$$

where C is a constant. The data covariance matrix, Σ , is the sum of the astrophysical covariance and the L2-regularized PLD covariance and is given by

$$\Sigma = \lambda X \lambda X^T + K \quad (5)$$

where K is the astrophysical covariance given by the EVEREST Gaussian process model, X is the matrix of PLD regressors (the design matrix), and λ is the prior covariance of the PLD weights (the regularization matrix), which we obtain by cross-validation⁸. As the transit shape and the duration of TRAPPIST-1 h are known², the only free parameter in the search is t_0 , the time of transit. We therefore evaluate \mathbf{m}_{t_0} multiple times, centering the transit model at each long cadence and computing the likelihood of the transit model fit as a function of cadence number. We then subtract these values from the log likelihood of the data with no transit model ($\mathbf{m}_{t_0} = 0$) and multiply by 2 to obtain the $\Delta\chi^2$ metric, which measures the decrease in the χ^2 value of the fitted light curve for a transit of TRAPPIST-1 h centred at each cadence. We also compute $\Delta\chi^2$ conditioned on the known ‘true’ transit depth of TRAPPIST-1 h, $d_0 = 0.00352 \pm 0.000326$:

$$\Delta\chi^2_{\text{cond}} = \Delta\chi^2 - \left(\frac{d - d_0}{\sigma_d} \right)^2 \quad (6)$$

where

$$d = \sigma_d^2 \mathbf{m}_{t_0}^T \Sigma^{-1} \mathbf{y} \quad (7)$$

is the maximum likelihood depth of the transit model and

$$\sigma_d^2 = \left(\mathbf{m}_{t_0}^T \Sigma^{-1} \mathbf{m}_{t_0} \right)^{-1} \quad (8)$$

is the variance of the depth estimate. Positive peaks in $\Delta\chi^2$ indicate features that are well described by the transit model, whereas positive peaks in $\Delta\chi^2_{\text{cond}}$ reveal features that are well described by the transit model with depth $d = d_0$. In Supplementary

Fig. 4, we show the two $\Delta\chi^2$ metrics across the full TRAPPIST-1 light curve after subtracting a transit model for planets TRAPPIST-1 b–g based on their Spitzer parameters. The strongest features in the $\Delta\chi^2$ plot are flares because these can be fitted out with an inverted transit model. When conditioning on the true depth of TRAPPIST-1 h, the significance of most of the flare features decreases, revealing the four peaks of TRAPPIST-1 h.

To assess the robustness of our detection, we compute the total $\Delta\chi^2_{\text{cond}}$ as a function of orbital period. Starting from the time of transit of TRAPPIST-1 h in the Spitzer dataset, we compute the times of transit in the K2 light curve for 500,000 values of the orbital period evenly spaced between 1 and 50 days and sum the values of $\Delta\chi^2_{\text{cond}}$ at each transit time to produce the total $\Delta\chi^2_{\text{p}}$. We sum these in two different ways. First, we linearly interpolate the grid of $\Delta\chi^2_{\text{cond}}$ to each transit time to obtain $\Delta\chi^2_{\text{p}}$ for perfectly periodic transits. Next, to allow for TTVs of up to 1 h, we take the largest value of $\Delta\chi^2_{\text{cond}}$ in the vicinity of each transit time and sum them for each period. We adopted a tolerance of two cadences, corresponding to maximum TTVs of 1 h. Our results are shown in Supplementary Fig. 5, where we plot the periodic $\Delta\chi^2_{\text{p}}$ and the $\Delta\chi^2_{\text{p}}$ allowing for TTVs. In both cases, the period of TRAPPIST-1 h (18.766 days) and its one-half and one-third period aliases emerge as the three strongest peaks. The peak at 18.766 days is the strongest signal in the period range constrained by the Spitzer transit² and confirms our detection of TRAPPIST-1 h.

Three-body angles. The mean longitude of a planet with orbital period P is an angular variable that progresses at a constant rate with respect to time t , which is measured from the time the planet passes a given reference direction:

$$\lambda = \frac{360^\circ}{P}t \quad (9)$$

with λ measured in degrees. For transiting planets, the reference direction is taken as the plane perpendicular to the observer's line of sight as the planet is progressing towards the transiting configuration. We assume orbits with negligible eccentricities¹¹, for which $\lambda = 90^\circ$ at transit mid-time, so that we may write:

$$\lambda = 360^\circ \left(\frac{1}{4} + \frac{t - T_n}{P} \right) \quad (10)$$

for each planet, where T_n is the time of transit of the n th planet. For a three-body resonance (p, q) , we may therefore express the three-body angle as:

$$\phi = 360^\circ \left[-p \frac{T_1}{P_1} + (p+q) \frac{T_2}{P_2} - q \frac{T_3}{P_3} + p \frac{t}{P_1} - (p+q) \frac{t}{P_2} + q \frac{t}{P_3} \right] \quad (11)$$

The state of a ϕ value is assessed when the individual transit times of three planets are taken near each other. For instance, for the transit times² $T_1 = 7,662.18747$, $T_2 = 7,665.35151$, $T_3 = 7,662.55463$ and $(p, q) = (1, 1)$, we compute $\phi = 177.4^\circ$ at $t = 7,664$ (BJD $-2,450,000$).

Tidal simulations. Tidal interactions with the star are important for all seven planets. We perform N-body simulations of the system, including an equilibrium tidal dissipation formalism^{43,44} using the Mercury-T code⁴⁵. We use orbital parameters from the discovery paper² and a period of TRAPPIST-1 h of 18.765 days (a near 2:3 resonance configuration with planet TRAPPIST-1 g). We consider the planets' spins to be tidally synchronized with small obliquities. This is justified because even if the age of the system is 400 Myr (a lower estimate for the age of TRAPPIST-1), planetary tides would have had time to synchronize the spins⁴⁶ (even when atmospheric tides are accounted for). We test different initial eccentricities and different values for the planets' dissipation factors (from 0.01 to 10 times the value for the Earth⁴⁷).

Our simulations show that the planets' orbital eccentricities are likely to be low. In just a few million years, all eccentricities decrease to <0.01 for dissipation factors ≥ 0.1 times the Earth's value. As a result of planet–planet interactions, the eccentricities do not decrease to zero, but instead reach an equilibrium value determined by the competition between tidal damping and planet–planet eccentricity excitation⁴⁸. All planets stay in resonance during the evolution towards tidal equilibrium. The small equilibrium eccentricities are sufficient to generate significant tidal heating. Assuming that the TRAPPIST-1 planets have a tidal dissipation equal to that of the Earth, we find that TRAPPIST-1 b might have a tidal heat flux similar to that of Io⁴⁹ ($\sim 3 \text{ W m}^{-2}$), with peaks at $>10 \text{ W m}^{-2}$ (corresponding to $\sim 10^4 \text{ TW}$) when the eccentricity oscillation is at its maximum. Planets c–e have tidal heat fluxes higher than the internal (primarily radioactive) heat flux of the Earth⁵⁰ ($\sim 0.08 \text{ W m}^{-2}$), but lower than Io's heat flux. TRAPPIST-1 f, g and h have a tidal heat flux lower than that of the Earth. Supplementary Fig. 6 shows a possible snapshot of the system's evolution over the course of 40 years. This very high flux could plausibly generate intense volcanism on the surfaces of the inner planets, with potential consequences for their internal structures.

Planet habitability. We calculate the minimum stellar flux required for liquid water with the LMD 1D/3D Global Climate Model⁵¹ using a synthetic spectrum of

TRAPPIST-1 based on its reported effective temperature (T_{eff}), surface gravity ($\log g$), metallicity and bolometric luminosity², obtaining a value of 300 W m^{-2} , which is 100 W m^{-2} higher than the planet's present day installation. Our results are in agreement with habitable zone boundaries computed for a 3,000 K star⁵². Assuming a zero albedo, we find that the equilibrium temperature of TRAPPIST-1 h is $173 \pm 4 \text{ K}$.

Whether or not TRAPPIST-1 h presently hosts an atmosphere is unclear. Given its radius measurement and a range of possible compositions (from pure water ice to pure iron), the mass of TRAPPIST-1 h is likely in the range $0.067\text{--}0.863 M_{\oplus}$; if TRAPPIST-1 h has an Earth-like composition, this value is $0.33 M_{\oplus}$ ⁵³. Assuming that TRAPPIST-1 h migrated to its current location quickly, the planet's low surface gravity could have led to the vigorous hydrodynamic escape of a primordial atmosphere in the first few 100 Myr after its formation, because at that time TRAPPIST-1 was considerably brighter and TRAPPIST-1 h would have been interior to the habitable zone^{54,55}. The presence of a subsequently outgassed atmosphere cannot be ruled out, however.

The surface of TRAPPIST-1 h could in theory harbour liquid water under such an outgassed atmosphere if it is rich in H_2 . Atmospheres composed of H_2 ^{56,57}, $\text{N}_2\text{--H}_2$ ⁵⁸ or $\text{CO}_2\text{--H}_2$ ^{59,60} have been shown to provide a sufficient greenhouse effect and internal heat blanketing for even lower instellation levels. Unless prevented by high-altitude clouds, transit spectroscopy with the Hubble Space Telescope may be able to reveal or rule out such an H_2 -rich atmosphere.

Stellar variability. To establish the rotation period of TRAPPIST-1, we clean the long cadence EVEREST light curve (Fig. 2) of remaining outliers, transits and flares. We iteratively fit and remove the low frequencies that remain in the light curve from the detrending process. To extract the rotation period, we calculate the discrete Fourier transform following a previously established method⁶¹ and proceed to fit the detected frequency with a non-linear least-squares method. The rotation period is determined to be 3.30 ± 0.14 days.

To determine the occurrence rate of stellar flares, we again take the EVEREST detrended long cadence light curve and remove transits and outliers. We require flares to have a peak emission 1% above the normalized continuum flux and two consecutive signals above the continuum. We detect a total of 19 flare events, corresponding to an average rate of 0.26 flares per day. A more refined determination of the flaring rate and energies requires an analysis of the short cadence data, which will be presented in a forthcoming paper.

Code availability. The kadenza code we use to generate pseudo-target pixel files for all K2 targets was downloaded from <https://doi.org/10.5281/zenodo.344973>. The code we use to generate and analyse the EVEREST light curves for TRAPPIST-1 is openly available at <https://github.com/rodluger/trappist1>. A static version of the repository has been archived at <https://doi.org/10.5281/zenodo.437548>.

Data availability. The K2 raw cadence data used in this study is available for download at https://archive.stsci.edu/missions/k2/c12_raw_cadence_data/. The pseudo-target pixel files for TRAPPIST-1 and its neighbouring stars generated with kadenza are archived at <https://doi.org/10.5281/zenodo.437876>. The detrended TRAPPIST-1 long cadence light curve and segments of the short cadence light curve in the vicinity of the transits of TRAPPIST-1 h are available at <https://doi.org/10.5281/zenodo.437548>. All other data that support the plots within this paper and other findings of this study are available from the corresponding author on reasonable request.

Received 11 March 2017; accepted 4 April 2017;
published 22 May 2017

References

- Gillon, M. *et al.* Temperate Earth-sized planets transiting a nearby ultracool dwarf star. *Nature* **533**, 221–224 (2016).
- Gillon, M. *et al.* Seven temperate terrestrial planets around the nearby ultracool dwarf star TRAPPIST-1. *Nature* **542**, 456–460 (2017).
- Quillen, A. C. Three-body resonance overlap in closely spaced multiple-planet systems. *Mon. Not. R. Astron. Soc.* **418**, 1043–1054 (2011).
- Howell, S. B. *et al.* The K2 mission: characterization and early results. *Publ. Astronom. Soc. Pacif.* **126**, 398–408 (2014).
- Quintana, E. V. *et al.* Pixel-level calibration in the Kepler Science Operations Center pipeline. *Proc. SPIE* **7740**, 77401X (2010).
- Demory, B.-O., Queloz, D., Alibert, Y., Gillen, E. & Gillon, M. Probing TRAPPIST-1-like systems with K2. *Astrophys. J. Lett.* **825**, L25 (2016).
- Luger, R. *et al.* EVEREST: pixel level decorrelation of K2 light curves. *Astron. J.* **152**, 100 (2016).
- Luger, R., Kruse, E., Foreman-Mackey, D., Agol, E. & Saunders, N. An update to the EVEREST K2 pipeline: short cadence, saturated stars, and Kepler-like photometry down to $K_p = 15$. Preprint at <https://arxiv.org/abs/1702.05488> (2017).

9. Peale, S. J. A primordial origin of the Laplace relation among the Galilean satellites. *Science* **298**, 593–597 (2002).
10. Rivera, E. J. *et al.* The Lick–Carnegie exoplanet survey: a Uranus-mass fourth planet for GJ 876 in an extrasolar Laplace configuration. *Astrophys. J.* **719**, 890–899 (2010).
11. Mills, S. M. *et al.* A resonant chain of four transiting, sub-Neptune planets. *Nature* **533**, 509–512 (2016).
12. MacDonald, M. G. *et al.* A dynamical analysis of the Kepler-80 system of five transiting planets. *Astron. J.* **152**, 105 (2016).
13. Baruteau, C. *et al.* in *Protostars and Planets VI* 4th edn (eds Beuther, H. *et al.*) 667–689 (Univ. Arizona Press, 2014).
14. Raymond, S. N., Barnes, R. & Mandell, A. M. Observable consequences of planet formation models in systems with close-in terrestrial planets. *Mon. Not. R. Astron. Soc.* **384**, 663–674 (2008).
15. Masset, F. S., Morbidelli, A., Crida, A. & Ferreira, J. Disk surface density transitions as protoplanet traps. *Astrophys. J.* **642**, 478–487 (2006).
16. Terquem, C. & Papaloizou, J. C. B. Migration and the formation of systems of hot super-Earths and Neptunes. *Astrophys. J.* **654**, 1110–1120 (2007).
17. Ogihara, M. & Ida, S. N-Body simulations of planetary accretion around M dwarf stars. *Astrophys. J.* **699**, 824–838 (2009).
18. Cossou, C., Raymond, S. N., Hersant, F. & Pierens, A. Hot super-Earths and giant planet cores from different migration histories. *Astron. Astrophys.* **569**, A56 (2014).
19. Fabrycky, D. C. *et al.* Architecture of Kepler's multi-transiting systems. II. New investigations with twice as many candidates. *Astrophys. J.* **790**, 146 (2014).
20. Izidoro, A. *et al.* Breaking the chains: hot super-Earth systems from migration and disruption of compact resonant chains. Preprint at <https://arxiv.org/abs/1703.03634> (2017).
21. Goździewski, K., Migaszewski, C., Panichi, F. & Szuszkiewicz, E. The Laplace resonance in the Kepler-60 planetary system. *Mon. Not. R. Astron. Soc.* **455**, L104–L108 (2016).
22. Pascucci, I. *et al.* A steeper than linear disk mass–stellar mass scaling relation. *Astrophys. J.* **831**, 125 (2016).
23. Matsumoto, Y., Nagasawa, M. & Ida, S. The orbital stability of planets trapped in the first-order mean-motion resonances. *Icarus* **221**, 624–631 (2012).
24. Ferraz-Mello, S., Rodrguez, A. & Hussmann, H. Tidal friction in close-in satellites and exoplanets: the Darwin theory re-visited. *Celest. Mech. Dynam. Astron.* **101**, 171–201 (2008).
25. Reid, N. & Hawley, S. *New Light on Dark Stars: Red Dwarfs, Low-Mass Stars, Brown Dwarfs* (Springer, 2013).
26. Newton, E. R. *et al.* The rotation and galactic kinematics of mid M dwarfs in the solar neighborhood. *Astrophys. J.* **821**, 93 (2016).
27. Aumer, M. & Binney, J. J. Kinematics and history of the solar neighbourhood revisited. *Mon. Not. R. Astron. Soc.* **397**, 1286–1301 (2009).
28. Burgasser, A. J. *et al.* The Brown Dwarf Kinematics Project (BDKP). IV. Radial velocities of 85 late-M and L dwarfs with MagE. *Astrophys. J. Suppl.* **220**, 18 (2015).
29. Hilton, E. J., Hawley, S. L., Kowalski, A. F. & Holtzman, J. The galactic M dwarf flare rate. *Astron. Soc. Pacif. Conf. Ser.* **448**, 197 (2011).
30. Deming, D. *et al.* Spitzer secondary eclipses of the dense, modestly-irradiated, giant exoplanet HAT-P-20b using pixel-level decorrelation. *Astrophys. J.* **805**, 132 (2015).
31. Howell, S. B. *et al.* Speckle imaging excludes low-mass companions orbiting the exoplanet host star TRAPPIST-1. *Astrophys. J. Lett.* **829**, L2 (2016).
32. Christiansen, J. L. *et al.* The derivation, properties, and value of Kepler's combined differential photometric precision. *Publ. Astronom. Soc. Pacif.* **124**, 1279–1287 (2012).
33. Aigrain, S., Hodgkin, S. T., Irwin, M. J., Lewis, J. R. & Roberts, S. J. Precise time series photometry for the Kepler-2.0 mission. *Mon. Not. R. Astron. Soc.* **447**, 2880–2893 (2015).
34. Aigrain, S., Parviainen, H. & Pope, B. J. S. K2SC: flexible systematics correction and detrending of K2 light curves using Gaussian process regression. *Mon. Not. R. Astron. Soc.* **459**, 2408–2419 (2016).
35. Ambikasaran, S., Foreman-Mackey, D., Greengard, L., Hogg, D. W. & O'Neil, M. Fast direct methods for Gaussian processes. *IEEE Trans. Pattern. Anal. Machine Intell.* **38**, 252–265 (2016).
36. Storn, R. & Price, K. Differential evolution — a simple and efficient heuristic for global optimization over continuous spaces. *J. Global Optim.* **11**, 341–359 (1997).
37. Mandel, K. & Agol, E. Analytic light curves for planetary transit searches. *Astrophys. J. Lett.* **580**, L171–L175 (2002).
38. Davenport, J. R. A. *et al.* Kepler flares. II. The temporal morphology of white-light flares on GJ 1243. *Astrophys. J.* **797**, 122 (2014).
39. Kovács, G., Zucker, S. & Mazeh, T. A box-fitting algorithm in the search for periodic transits. *Astron. Astrophys.* **391**, 369 (2002).
40. Gillon, M. *et al.* The TRAPPIST survey of southern transiting planets. I. Thirty eclipses of the ultra-short period planet WASP-43 b. *Astron. Astrophys.* **542**, A4 (2012).
41. Claret, A. & Bloemen, S. Gravity and limb-darkening coefficients for the Kepler, CoRoT, Spitzer, uvby, UBVRJHK, and Sloan photometric systems. *Astron. Astrophys.* **529**, 75 (2011).
42. Foreman-Mackey, D. *et al.* A systematic search for transiting planets in the K2 data. *Astrophys. J.* **806**, 215 (2015).
43. Eggleton, P. P., Kiseleva, L. G. & Hut, P. The equilibrium tide model for tidal friction. *Astrophys. J.* **499**, 853–870 (1998).
44. Leconte, J., Chabrier, G., Baraffe, I. & Levrard, B. Is tidal heating sufficient to explain bloated exoplanets? Consistent calculations accounting for finite initial eccentricity. *Astron. Astrophys.* **516**, A64 (2010).
45. Bolmont, E., Raymond, S. N., Leconte, J., Hersant, F. & Correia, A. C. M. Mercury-T: a new code to study tidally evolving multi-planet systems. Applications to Kepler-62. *Astron. Astrophys.* **583**, A116 (2015).
46. Leconte, J., Wu, H., Menou, K. & Murray, N. Asynchronous rotation of Earth-mass planets in the habitable zone of lower-mass stars. *Science* **347**, 632–635 (2015).
47. Neron de Surgy, O. & Laskar, J. On the long term evolution of the spin of the Earth. *Astron. Astrophys.* **318**, 975–989 (1997).
48. Bolmont, E. *et al.* Tidal dissipation and eccentricity pumping: implications for the depth of the secondary eclipse of 55 Cancri e. *Astron. Astrophys.* **556**, A17 (2013).
49. Spencer, J. R., Jessup, K. L., McGrath, M. A., Ballester, G. E. & Yelle, R. Discovery of gaseous S₂ in Io's Pele plume. *Science* **288**, 1208–1210 (2000).
50. Davies, J. H. & Davies, D. R. Earth's surface heat flux. *Solid Earth* **1**, 5–24 (2010).
51. Turbet, M. *et al.* The habitability of Proxima Centauri b. II. Possible climates and observability. *Astron. Astrophys.* **596**, A112 (2016).
52. Kopparapu, R. K. *et al.* Habitable zones around main-sequence stars: new estimates. *Astrophys. J.* **765**, 131 (2013).
53. Sotin, C., Grasset, O. & Mocquet, A. Mass radius curve for extrasolar Earth-like planets and ocean planets. *Icarus* **191**, 337–351 (2007).
54. Luger, R. *et al.* Habitable evaporated cores: transforming mini-Neptunes into super-Earths in the habitable zones of M dwarfs. *Astrobiology* **15**, 57–88 (2015).
55. Luger, R. & Barnes, R. Extreme water loss and abiotic O₂ buildup on planets throughout the habitable zones of M dwarfs. *Astrobiology* **15**, 119–143 (2015).
56. Stevenson, D. J. Life-sustaining planets in interstellar space? *Nature* **400**, 32 (1999).
57. Pierrehumbert, R. & Gaidos, E. Hydrogen greenhouse planets beyond the habitable zone. *Astrophys. J.* **734**, L13 (2011).
58. Wordsworth, R. & Pierrehumbert, R. Hydrogen–nitrogen greenhouse warming in Earth's early atmosphere. *Science* **339**, 64–67 (2013).
59. Ramirez, R. M. & Kaltenegger, L. A volcanic hydrogen habitable zone. *Astrophys. J. Lett.* **837**, L4 (2017).
60. Wordsworth, R. *et al.* Transient reducing greenhouse warming on early Mars. *Geophys. Res. Lett.* **44**, 665–671 (2017).
61. Kurtz, D. W. An algorithm for significantly reducing the time necessary to compute a discrete Fourier transform periodogram of unequally spaced data. *Mon. Not. R. Astron. Soc.* **213**, 773 (1985).

Acknowledgements

This paper includes data collected by the K2 mission. Funding for the K2 mission is provided by the NASA (National Space and Aeronautical Administration) Science Mission directorate. This research has made use of NASA's Astrophysics Data System, the SIMBAD database and VizieR catalogue access tool operated at Centre de Données astronomiques de Strasbourg, Strasbourg, France. The data presented in this paper were obtained from the Mikulski Archive for Space Telescopes. R.L. and E.A. acknowledge support from NASA grant NNX14AK26G and from the NASA Astrobiology Institute's Virtual Planetary Laboratory Lead Team, funded through the NASA Astrobiology Institute under solicitation NNN12ZDA002C and Cooperative Agreement Number NNA13AA93A. E.A. acknowledges support from NASA grant NNX13AF62G and National Science Foundation grant AST-1615315. E.K. acknowledges support from a National Science Foundation Graduate Student Research Fellowship. B.-O.D. acknowledges support from the Swiss National Science Foundation in the form of a Swiss National Science Foundation Professorship (PP00P2-163967). E.B. acknowledges funding by the European Research Council through ERC grant SPIRE 647383. D.L.H. acknowledges financial support from the UK Science and Technology Facilities Council. M.S. and K.H. acknowledge support from the Swiss National Science Foundation. A.B. acknowledges funding support from the National Science Foundation under award no. AST-1517177 and NASA under grant no. NNX15AI75G. J.L. acknowledges funding from the European Research Council under the European Unions Horizon 2020 research and innovation programme (grant agreement no. 679030/WHIPLASH). M.G., E.J. and V.V.G. are Fonds National de la Recherche Scientifique (F.R.S.-FNRS) Research

Associates. S.N.R. thanks the Agence Nationale pour la Recherche for support via grant ANR-13-BS05-0003-002 (grant MOJO). The research leading to these results has received funding from the European Research Council under the FP/2007-2013 European Research Council Grant Agreement no. 336480 and from the Actions de Recherche Concertée (ARC) grant for Concerted Research Actions, financed by the Wallonia–Brussels Federation. S.B.H. wrote science cases to the K2 project office to include TRAPPIST-1 in the campaign 12 field and to make the raw data public upon downlink. D.F.M. is a Sagan Fellow.

Author contributions

R.L. and M.S. led the detrending efforts with EVEREST and the Gaussian process-based pipeline, with inputs from E.A., J.G.I, E.K. and D.F.M. R.L. performed the preliminary manual search for transits of TRAPPIST-1 h and the $\Delta\chi^2$ search, with input from E.A., E.K. and D.F.M. S.L.G. took care of the K2 data handling. B.-O.D. led the collaboration, wrote the K2 proposal and performed an independent transit search and Markov Chain Monte Carlo analysis of the K2 dataset. E.A. and D.F. led the dynamics and architecture of the system with inputs from S.N.R. and B.-O.D. E.B. took care of the tidal simulations. C.S.F. V.V.G., A.B., D.L.H. and B.M.M. conducted the work on stellar properties and variability and determined the stellar rotation period. S.N.R. led the formation and migration section. F.S., J.L. and M.T. worked on the atmospheric nature

of TRAPPIST-1 h. G.B. and T.B. helped with the handling of the uncalibrated K2 fits files. Figures were prepared by R.L., A.H.M.J.T., J.G.I., E.B and E.K. M.G., E.J., A.H.M.J.T., L.D., J.d.W, S.L., Y.A., Z.B., P.M., K.H. and D.Q. contributed to the discovery and characterization of the TRAPPIST-1 system. All authors participated in the writing and commented on the paper.

Additional information

Supplementary information is available for this paper.

Reprints and permissions information is available at www.nature.com/reprints.

Correspondence and requests for materials should be addressed to R.L.

How to cite this article: Luger, R. *et al.* A seven-planet resonant chain in TRAPPIST-1. *Nat. Astron.* **1**, 0129 (2017).

Publisher's note: Springer Nature remains neutral with regard to jurisdictional claims in published maps and institutional affiliations.

Competing interests

The authors declare no competing financial interests.